On-chip silicon optical phased array for two-dimensional beam steering

David Kwong,[1,*] Amir Hosseini,[2] John Covey,[1] Yang Zhang,[1] Xiaochuan Xu,[1] Harish Subbaraman,[2] and Ray T. Chen[1,3]

[1]*Microelectronics Research Center, Department of Electrical and Computer Engineering, University of Texas at Austin, 10100 Burnet Rd., Austin, Texas 78758, USA*

[2]*Omega Optics, Inc, 10306 Sausalito Dr., Austin, Texas 78759, USA*

[3]*e-mail: raychen@uts.cc.utexas.edu*

**Corresponding author: david.kwong@utexas.edu*

Received August 14, 2013; revised December 5, 2013; accepted December 8, 2013; posted January 3, 2014 (Doc. ID 195791); published February 10, 2014

A 16-element optical phased array integrated on chip is presented for achieving two-dimensional (2D) optical beam steering. The device is fabricated on the silicon-on-insulator platform with a 250 nm silicon device layer. Steering is achieved via a combination of wavelength tuning and thermo-optic phase shifting with a switching power of $P_\pi =$ 20 mW per channel. Using a silicon waveguide grating with a polycrystalline silicon overlay enables narrow far field beam widths while mitigating the precise etching needed for conventional shallow etch gratings. Using this system, 2D steering across a 20° × 15° field of view is achieved with a sidelobe level better than 10 dB and with beam widths of 1.2° × 0.5°.

OCIS codes: (130.3120) Integrated optics devices; (250.5300) Photonic integrated circuits; (280.3640) Lidar.
http://dx.doi.org/10.1364/OL.39.000941

Optical-phased arrays (OPAs) can provide agile and precise free-space optical beam steering free of any moving parts [1]. Potential applications include free-space board-to-board optical interconnects and light detection and ranging. By using the silicon-on-insulator (SOI) platform and leveraging existing CMOS process technologies, complex photonic circuits can be easily integrated on chip to reduce both the size and packaging complexity of silicon photonic devices. Combined with the high optical damage threshold of silicon at 1–4 GW/cm^2 [2], this enables compact silicon-based OPAs with high power handling capabilities to be realized.

We have previously achieved steering in the horizontal direction using a thermo-optically tuned 12-channel unequally spaced OPA [3]. However, for many applications two-dimensional (2D) steering is necessary. Recent silicon-based OPAs have used a combination of wavelength tuning and thermo-optic (TO) phase shifting to achieve 2D optical beam steering [4–6]. Free-space emission [7] was achieved using shallow etched surface gratings to reduce a silicon grating's inherently large index contrast, allowing for narrower longitudinal beam widths via larger emission apertures. However, precise control of the etch depth is required for shallow etched gratings. Van Acoleyen *et al.* achieved a longitudinal beam width of ~2.5° by shallow etching 70 nm of the 220 nm silicon device layer [4]. Doylend *et al.* used a significantly thicker silicon layer of 500 nm and shallow etched the output gratings by 75 nm to achieve a longitudinal beam width of 0.6° [5]. While using a thicker silicon layer can reduce the index contrast for a given etch depth, a significant disadvantage is that the power consumption for TO phase shifting is increased due to the increased waveguide volume. In addition, as the silicon thickness now supports multiple vertical modes, rib waveguides are needed for single-mode operation, thereby adding additional patterning steps, which increases cost and complexity. Moreover, the etch depth still must be precisely controlled. It is desirable to use a free-space coupling structure that can still provide narrow far field beam widths while eliminating the need for precise shallow etching and still adhering to silicon device thicknesses of ~250 nm that only support a single vertical mode.

In this work we demonstrate 2D beam steering using both wavelength tuning and TO phase shifting with a 16-element OPA fabricated on SOI with a 250 nm silicon device layer. The output coupling structure incorporates a polycrystalline silicon (polysilicon) overlay with an oxide etch stop layer to realize narrow far field beam widths while eliminating the need for precise shallow etching. A schematic of the device is shown in Fig. 1(a). The device consists of several key components: a wideband

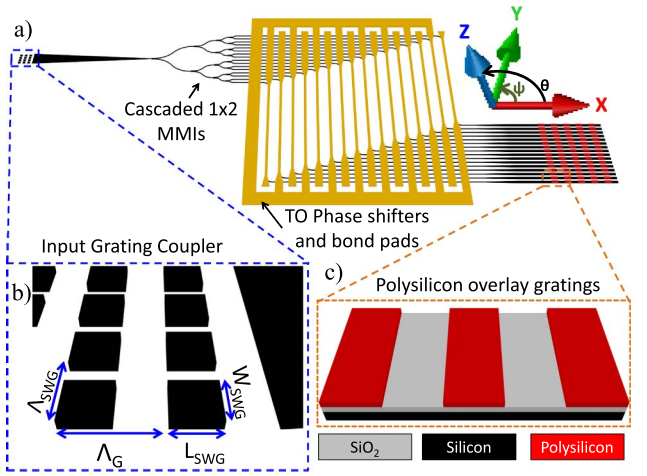

Fig. 1. (a) Schematic of the overall device with (b) wideband subwavelength grating coupler and (c) waveguide grating with polysilicon overlay and oxide etch stop layer. Note that the metal phase shifters are directly over the silicon waveguide separated by 1 μm of oxide. Horizontal (longitudinal) steering refers to beam steering in the x–y(x–z) plane and the steering angle is represented by $\psi(\theta)$.

fiber to waveguide grating coupler, cascaded 1×2 multimode interference (MMI) optical beam splitters, metal TO phase shifters, and finally the output grating couplers with a polysilicon overlay. All of the photonic components are designed for transverse electric (TE) polarization.

Light is first coupled into the photonic circuit using the input grating coupler. For this application, we have used subwavelength nanostructures (SWNs) in the grating couplers to reduce the index contrast in silicon gratings [8–11]. A schematic of the SWN grating coupler is shown in Fig. 1(b). The SWN can be treated as a homogeneous medium according to effective medium theory (EMT) when the subwavelength period Λ_{SWG} is below the wavelength in the material [8,9,12]. The refractive index of the SWN region n_{SWG} is an intermediate value between a high index material ($n_{high} = n_{si} = 3.48$) and low index material ($n_{low} = n_{air} = 1$) and is a function of the fill factor, which is defined as W_{SWG}/Λ_{SWG}.

As our wavelength tuning range is from 1480 to 1580 nm, it is important to utilize a grating coupler with a sufficiently large bandwidth. This can be achieved by lowering the average effective index of the grating region in order to reduce waveguide dispersion [11], such that the high index region of the grating is the subwavelength region and the low index region is the cladding. Using 2D finite-difference time-domain (FDTD) simulations, we optimize the grating coupler to arrive at a design of grating period $\Lambda_G = 1.3$ μm with $L_{SWG} = 728$ nm and $n_{SWG} = 2.15$. We then use EMT theory to choose the subwavelength period $\Lambda_{SWG} = 360$ nm with $W_{SWG} = 290$ nm.

Cascaded 1×2 MMI couplers are used to split the input light into 16 uniform outputs. The 16 MMI outputs with 4 μm spacing are separated to 200 μm spacing for TO phase shifting [see Fig. 1(a)] and then back to 4 μm for the OPA output. By keeping the optical path length the same for all array elements throughout the rest of the device, we allow for the array elements to have the same phase at the output, thereby ensuring the beam is steered at 0° without any thermal tuning.

Phase shifting is achieved using the TO effect in silicon ($dn/dT = 1.86\text{E}-4\ \text{K}^{-1}$), by placing metal heaters above the waveguide. The waveguide is separated from the metal heater by 1 μm of silicon dioxide, which is sufficiently thick to prevent large absorption losses by isolating the guided mode from the metal. There are 16 independently controlled phase shifters to achieve resets with modulo 2π phase shifts.

The output grating coupler array element shown in Fig. 1(c) is an 800 nm wide silicon waveguide covered with 20 nm of silicon dioxide, which serves not only as an etch mask for patterning the silicon waveguide but also as an etch stop layer for patterning the 20 nm thick polysilicon overlay due to the high selectivity of the etch between silicon and silicon dioxide. This etch stop layer significantly relaxes the fabrication process in creating these surface gratings. From 2D FDTD we find the upward coupling efficiency to be ~ – 1.7 dB.

The SOI has a 250 nm silicon device layer with 3 μm buried oxide thickness. First, 20 nm of silicon dioxide was deposited using plasma enhanced chemical vapor deposition. Next, 20 nm of high-quality amorphous silicon film was deposited using low pressure chemical vapor deposition (LPCVD) and was subsequently annealed at 600°C for 10 h, similar to our previous process in demonstrating ultralow-loss polysilicon films [13]. Standard electron-beam lithography and reactive ion etching (RIE) were used to define the polysilicon grating lines, with the RIE etch stopping on the oxide layer below it due to the high selectivity of the silicon etch. E-beam lithography and RIE were used again to pattern the silicon device layer. A top-down scanning electron microscope (SEM) of the fiber to waveguide grating coupler is shown in Fig. 2(a). A tilted SEM of the fabricated waveguide grating with the polysilicon overlay is shown in Fig. 2(b). Afterward, 1 μm of LPCVD silicon dioxide was deposited for top cladding and passivation. The TO phase shifters were then patterned using lift-off of Cr/Au (5/150 nm). Finally, the chip was mounted on a chip carrier to be plugged into a breadboard. Gold ball bonding was used to connect the bond pads on the chip with the electrical connections on the chip carrier. A microscope picture of the completed device, which measures 1 mm × 9 mm, is shown in Fig. 2(c), and the wire-bonded device on the chip carrier and breadboard is shown in Fig. 2(d).

The transmission spectrum of a single grating coupler is shown in Fig. 3(a), with a maximum coupling efficiency of $\eta_{max} = -5.4$ dB at a central wavelength of $\lambda_c = 1555$ nm and a 3 dB bandwidth of 124 nm, which is large enough to cover our wavelength tuning range.

To characterize the OPA beam steering and far field, the testing setup in Fig. 3(b) is used. A tunable external cavity laser is used to couple light into the device via the input grating coupler. The emitted light from the output grating array is directly imaged onto the InGaAs IR camera that is suspended above the device. A 16-channel independently controlled voltage source is used to control the phase of each array element. A

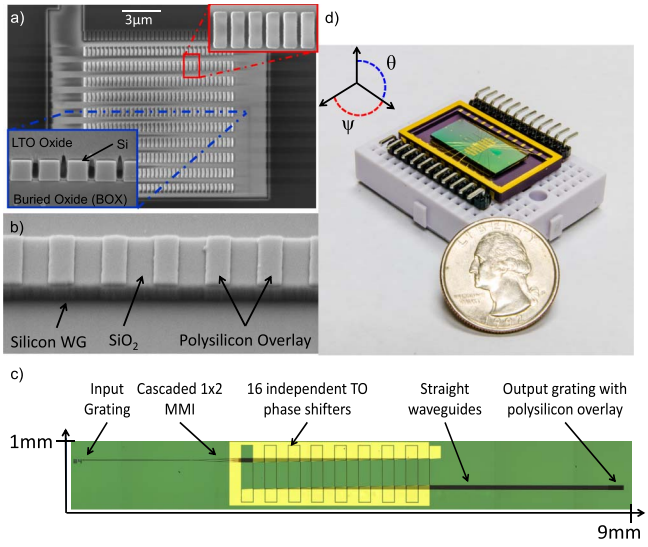

Fig. 2. (a) Top-down SEM of the SWN grating coupler. Insets show magnified view (top right) and cross-sectional view with oxide cladding (bottom left). (b) SEM of a single waveguide grating with polysilicon overlay and oxide etch stop layer. (c) Microscope picture of the completed device. (d) Picture of the wire-bonded device on the chip carrier plugged into the breadboard.

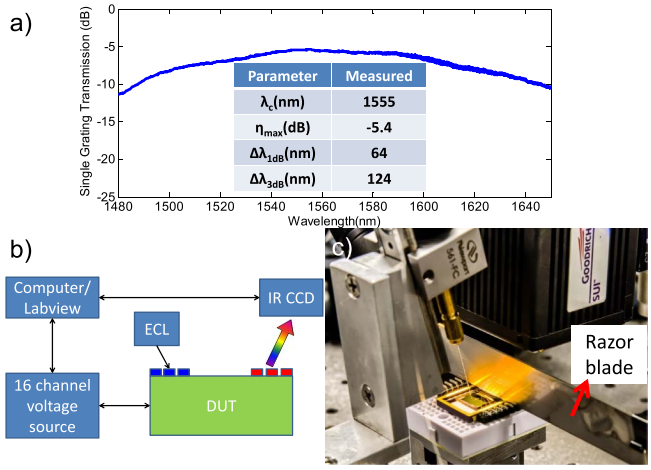

Fig. 3. (a) Coupling efficiency of the wideband subwavelength grating coupler. (b) Schematic of the testing setup used to achieve 2D beam steering using the OPA. (c) Photograph of the testing setup showing the razor blade to block reflected light from entering the IR camera.

LabVIEW-equipped computer is used to optimize the applied voltage of each channel with continuous feedback from the IR camera in order to achieve thermo-optically tuned beam steering. The figure of merit to be optimized is the emitted power efficiency (PE), which is the power directed into the desired steering angle ψ (within one beam width) compared with the total emitted power.

Before achieving active beam steering, we first use wavelength tuning to characterize the steering of a single waveguide grating, which forms the steering envelope of the array. The steering achieved by wavelength tuning is governed by the phase matching condition and is given by $\sin(\theta) = (n_{\text{eff,avg}} \cdot \Lambda - \lambda)/(\Lambda \cdot n_{\text{clad}})$, where θ is the steered angle in the longitudinal direction, $n_{\text{eff,avg}}$ is the average effective index of the grating, Λ is the grating period, λ is the free-space wavelength, and $n_{\text{clad}} = 1$ is the refractive index of the cladding, where θ is observed. IR images of the steered beam as the wavelength is changed from 1480 to 1580 nm in 10 nm steps are shown in Fig. 4(a), along with the longitudinal beam profiles in Fig. 4(b). The steering angle and full width at half-maximum (FWHM) beam width are shown in Fig. 4(c). A total of 15° of steering was achieved with wavelength tuning, with an average beam width of ~0.5°, which is the narrowest beam width achieved to date with integrated waveguide grating and indicates that our polysilicon overlay with the oxide etch stop layer is a more effective alternative to shallow etching. The output waveguide gratings are 260 μm long. Given the exponential radiation profile, the effective grating length is estimated to be 75 μm.

We also characterize the phase shifting properties of the metal heater by using a Mach–Zehnder interferometer (MZI) with the same waveguide and heater dimensions as in the actual OPA. The switching power required for a π phase shift was determined to be $P_\pi = 20$ mW, as shown in Fig. 5(a). Figure 5(b) shows the transient response of the phase shifters was characterized, and a 10%–90% rise time was experimentally determined to be $t_{\text{rise}} = 48$ μs, corresponding to a 3 dB modulation bandwidth of 7.3 kHz.

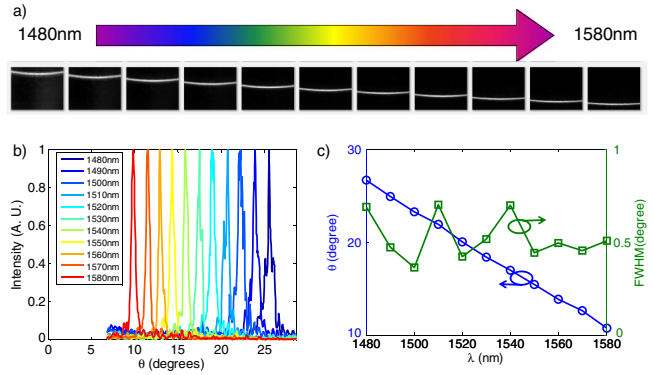

Fig. 4. (a) IR images of the single waveguide grating with polysilicon overlay as the wavelength is tuned from 1480 to 1580 nm. (b) Longitudinal beam profiles in θ of the steered beams. (c) Steering angle and FWHM beam width of the steered beam.

With the phase tuning efficiency of the heater characterized, it is now possible to achieve phase shifting in the horizontal direction ψ. The steering in ψ for a uniform array is determined by $\sin\psi = (\lambda\phi)/(2\pi d)$, where ϕ is the uniform phase difference between adjacent array elements, λ is the free-space wavelength, and d is the element spacing. However, in the 16-element OPA, fabrication imperfections in the heaters can result in deviations of P_π from the previously determined value. It was therefore impractical to use the MZI heater characterization results for beam steering. A LabVIEW system with constant feedback between the 16-channel voltage source and the IR camera therefore provides a more feasible approach to beam steering.

At a wavelength of 1550 nm, the OPA far field and line profile without any thermal phase shifting are shown in Figs. 6(a) and 6(b), respectively. The presence of the mainlobe at ~9° and additional sidelobes indicates phase errors are present, despite attempts being made to reduce the phase errors through the use of cascaded 1×2 MMIs and equalized optical path lengths. We believe that small, cumulative fabrication imperfections in the waveguides are inducing these phase errors. Therefore, thermal tuning is needed to correct these phase errors by using the LabVIEW feedback control system. PE is calculated from the measured far field and maximized by optimizing the voltages applied to the electrodes.

The OPA far field and line profile after thermal tuning with a horizontal beam width of 1.1° are shown in Figs. 6(c) and 6(d). They show good agreement with the theoretical value of 1.2°. Using the LabVIEW feedback control system, we steered the beam to a maximum angle of 19.6° in the longitudinal (ψ) direction, with a

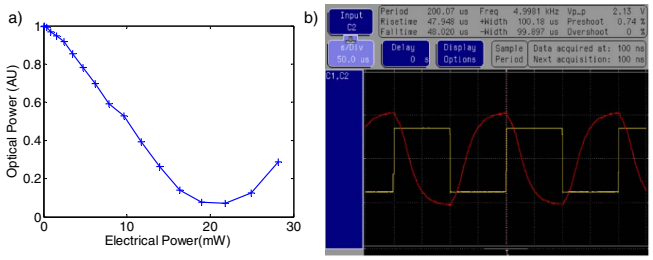

Fig. 5. (a) MZI transmission spectrum vs. electrical power to TO phase shifters. (b) Oscilloscope screenshot of MZI.

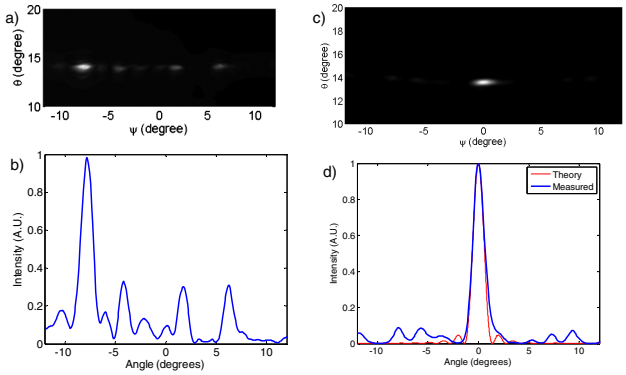

Fig. 6. (a) OPA far field and (b) line profile without thermal tuning. (c) OPA far field and (d) line profile after thermal tuning.

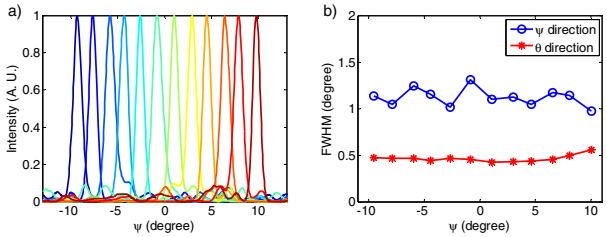

Fig. 7. (a) 2D beam steering around a $20° \times 15°$ field of view with SLL better than 10 dB and (b) beam widths of $1.2° \times 0.5°$.

sidelobe level (SLL) of more than 10 dB throughout the steering range, as shown in Fig. 7(a). In addition, the horizontal and longitudinal beam widths are shown in Fig. 7(b), with an average horizontal beam width of ~1.2° and average longitudinal beam width of ~0.5°, which matches well with the single waveguide grating results.

Combined with wavelength tuning, it is now possible to achieve 2D beam steering. This 2D beam steering can be seen in Fig. 8, in which the beam is steered along the perimeter of the entire field of view, which is a rectangular area that is 20° in θ by 15° in ψ. The far fields of these steered beams are shown overlaid upon each other and show an SLL better than 10 dB, with beam widths of $1.2° \times 0.5°$.

In summary, we have demonstrated an integrated optical beam steering system using a 16-element optical phased array fabricated on SOI. 2D beam steering is achieved using a combination of wavelength tuning and TO phase shifting, with a switching power of $P_\pi =$ 20 mW per channel. The output coupling to free space is achieved using a thin polysilicon overlay. Compared to conventional shallow etched gratings, this structure eliminates the need for precisely controlled etching due to the built-in oxide etch stop layer, thereby greatly simplifying the fabrication complexity. With this device, 2D steering across a $20° \times 15°$ field of view has been demonstrated, with an SLL better than 10 dB and $1.2° \times 0.5°$ beam widths.

The authors acknowledge the Multidisciplinary University Research Initiative (MURI) program through the Air Force Office of Scientific Research (AFOSR), contract no. FA 9550-08-1-0394, monitored by Dr. Gernot S. Pomrenke.

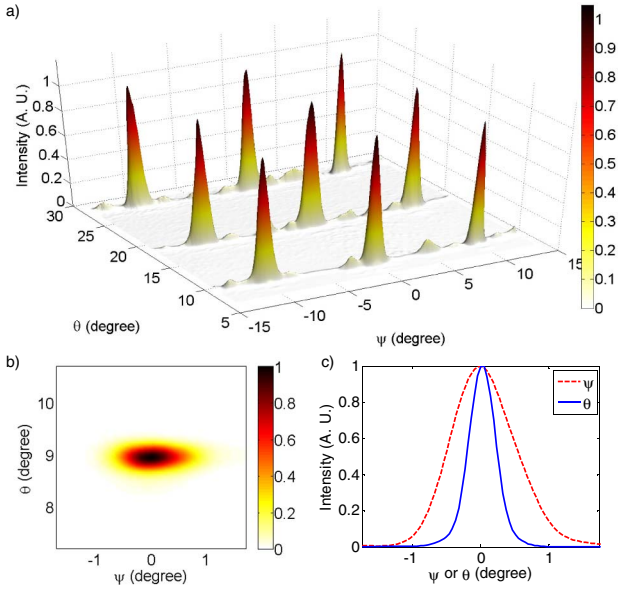

Fig. 8. (a) 2D beam steering around a $20° \times 15°$ field of view with SLL better than 10 dB. (b) Far field radiation pattern and (c) beam profiles of one of the steered beams showing beam widths of $1.2° \times 0.5°$.

References

1. P. F. McManamon, P. J. Bos, M. J. Escuti, J. Heikenfeld, S. Serati, H. Xie, and E. A. Watson, Proc. IEEE **97**, 1078 (2009).
2. B. Jalali, V. Raghunathan, R. Shori, S. Fathpour, D. Dimitropoulos, and O. Stafsudd, IEEE J. Sel. Top. Quantum Electron. **12**, 1618 (2006).
3. D. Kwong, A. Hosseini, Y. Zhang, and R. T. Chen, Appl. Phys. Lett. **99**, 051104 (2011).
4. K. Van Acoleyen, W. Bogaerts, J. Jágerská, N. Le Thomas, R. Houdré, and R. Baets, Opt. Lett. **34**, 1477 (2009).
5. J. K. Doylend, M. Heck, J. T. Bovington, J. D. Peters, L. Coldren, and J. Bowers, Opt. Express **19**, 21595 (2011).
6. J. Sun, E. Timurdogan, A. Yaacobi, E. S. Hosseini, and M. R. Watts, Nature **493**, 195 (2013).
7. P. Cheben, S. Janz, B. Lamontagne, and D.-X. Xu, "Optical off-chip interconnects in multichannel planar waveguide devices," U.S. patent application 2005/0141808 A1 (December 21, 2004).
8. R. Halir, P. Cheben, S. Janz, D.-X. Xu, Í. Molina-Fernández, and J. G. Wangüemert-Pérez, Opt. Lett. **34**, 1408 (2009).
9. X. Xu, H. Subbaraman, J. Covey, D. Kwong, A. Hosseini, and R. T. Chen, Appl. Phys. Lett. **101**, 031109 (2012).
10. R. Halir, P. Cheben, J. Schmid, R. Ma, D. Bedard, S. Janz, D.-X. Xu, A. Densmore, J. Lapointe, and Í. Molina-Fernández, Opt. Lett. **35**, 3243 (2010).
11. X. Chen, K. Xu, Z. Cheng, C. K. Fung, and H. K. Tsang, Opt. Lett. **37**, 3483 (2012).
12. X. Chen and H. K. Tsang, Opt. Lett. **36**, 796 (2011).
13. D. Kwong, J. Covey, A. Hosseini, Y. Zhang, X. Xu, and R. T. Chen, Opt. Express **20**, 21722 (2012).